TURBULENT MHD FREE SURFACE FLOW IN SQUARE CONTAINERS

H. A. Navarro
Departamento de Estatística, Matemática Aplicada e Computação, Instituto de Geociências e Ciências Exatas,
Av. 24-A, 1515 - C.P. 178 - 13506-700, Rio Claro, SP, Brazil
helio@rc.unesp.br

V. G. Ferreira
Departamento de Ciências de Computação e Estatística, Instituto de Ciências Matemáticas e de Computação,
Av. Trabalhador São Carlense, 400, C.P. 668, 13251-900, São Carlos, SP, Brazil
pvgf@lcad.icmc.sc.usp.br

A. Castelo
Departamento de Ciências de Computação e Estatística, Instituto de Ciências Matemáticas e de Computação,
Av. Trabalhador São Carlense, 400, C.P. 668, 13251-900, São Carlos, SP, Brazil
castelo@lcad.icmc.sc.usp.br

J. A. Cuminato
Departamento de Ciências de Computação e Estatística, Instituto de Ciências Matemáticas e de Computação,
Av. Trabalhador São Carlense, 400, C.P. 668, 13251-900, São Carlos, SP, Brazil
jacumina@lcad.icmc.sc.usp.br

N. Mangiavacchi
Departamento de Engenharia Mecânica, Universidade do Estado do Rio de Janeiro, UERJ, Rua São Francisco
Xavier, 524, 20550-900, Rio de Janeiro, RJ, Brazil
norberto@uerj.br

F. M. Federson
Departamento de Ciências de Computação e Estatística, Instituto de Ciências Matemáticas e de Computação,
Av. Trabalhador São Carlense, 400, C.P. 668, 13251-900, São Carlos, SP, Brazil
fernando@icmc.usp.br

M. F. Tomé
Departamento de Ciências de Computação e Estatística, Instituto de Ciências Matemáticas e de Computação,
Av. Trabalhador São Carlense, 400, C.P. 668, 13251-900, São Carlos, SP, Brazil
murilo@lcad.icmc.usp.br

__Abstract.__ This paper deals with numerical solution of two-dimensional turbulent MHD incompressible free-surface fluid flow problems. The numerical method employed to solve the conservation equations is an extension of GENSMAC: a finite-difference marker-and-cell technique for the numerical solution of incompressible free-surface flows using the velocity-pressure formulation. The Maxwell and the Prandtl mixing length turbulent Navier-Stokes equations are solved in open square containers with electromagnetic coils aligned externally on their sides. These produce an alternating magnetic field, creating eddy currents within the molten metal and, consequetly, a Lorentz force which drives the fluid. When the frequency of the field is low, the Lorentz force penetrates far into the liquid and may introduce a turbulent fluid flow and a good mixing. Results of the simulations are presented for electromagnetic stirring of steel.

__keywords:__ turbulent electromagnetic stirring, free-surface MHD fluid flow, finite-difference formulation.

1. Introduction

There are several industrial applications that arise from a rotating magnetic field on a container of liquid metal: the continuous stirring of castings can lead to finer grain structure and centrifuging can be used to remove impurities. Historically, the mechanism of electromagnetic stirring was observed at the beginning of the century in an experiment conduced by Northrup, 1907 when surface agitation was detected on a sample of

liquid sodium situated between alternating current electrodes. In this instance, the force causing the agitation was due primarily to the special geometry of the container which created a "pinching" effect on the electrical and magnetic fields which in turn determined the nature of the Lorentz force within the liquid metal.

The pioneering work of Moffatt, 1965 was later extended by several authors. Sneyd, 1971 considered a circular cylindrical container of conducting fluid in an alternating field; Nigam, 1969 examined a spherical container of conducting fluid in a rotating magnetic field; Richardson, 1974 examined the stability of Dahlberg's solution concluding that instability would occur for very small magnetic field strengths; and Sneyd, 1979 showed that in containers of any shape the rate of vorticity generation includes both constant and oscillatory terms with complex flows developing in the viscous-magnetic boundary layer.

Fluid flow applications must solve not only Maxwell's equations for the electromagnetics, but also Navier-Stokes' equations governing the flow itself. In a fluid flow application a balance must be set between the computational requirements of the numerical fluid solver and the demands of the electromagnetic solver. This paper deals with the numerical solution of two-dimensional turbulent MHD incompressible free-surface fluid flow problems. The numerical method employed to solve the conservation equations is an extension of GENSMAC: a finite-difference marker-and-cell technique for the numerical solution of incompressible free-surface flows using the velocity-pressure formulation.

2. Governing equations

Maxwell's equations for a linear homogeneous material are

$$\nabla \cdot \mathbf{B} = 0, \tag{1}$$

$$\nabla \times \mathbf{B} = \mu_0 \mathbf{J}, \tag{2}$$

$$\nabla \cdot \mathbf{E} = \frac{\rho_c}{\epsilon_0}, \tag{3}$$

$$\nabla \times \mathbf{E} = -\frac{\partial \mathbf{B}}{\partial t}, \tag{4}$$

where $\mathbf{E}$, $\mathbf{B}$, and $\mathbf{J}$ are, respectively, the electric field, the magnetic induction, and the electric current density. In Eqs. (1)-(4), ρ_c is the net electric charge, ϵ_0 is the electric permittivity of the material, and μ_0 is the magnetic permeability of the material. In the case of liquid steel, these material properties are assumed constant and equal to those of free space (Davidson and Hunt, 1987).

The constitutive equation relating the current density to the applied fields in a fluid with velocity $\mathbf{V}$ is the Ohm's law

$$\mathbf{J} = \sigma(\mathbf{E} + \mathbf{V} \times \mathbf{B}), \tag{5}$$

where σ is the electrical conductivity that is assumed scalar (isotropy). The motion of MHD incompressible viscous fluid flows is described by mass conservation and Navier-Stokes equations

$$\nabla \cdot \mathbf{V} = 0, \tag{6}$$

$$\frac{\partial \mathbf{V}}{\partial t} + \nabla \cdot (\mathbf{V}\mathbf{V}) = -\frac{1}{\rho}\nabla p^* + \nu \nabla^2 \mathbf{V} + \mathbf{G} + \mathbf{J} \times \mathbf{B}, \tag{7}$$

where ν is the constant kinematic viscosity, ρ is the constant density, p^* is the pressure field, and $\mathbf{G}$ is the gravitational field. Equations (2) and (5) couple the Maxwell equations to the turbulent Navier-Stokes equations. These equations together with the continuity equation are

$$\nabla \cdot \mathbf{u} = 0, \tag{8}$$

$$\nabla \cdot \mathbf{b} = 0, \tag{9}$$

$$\frac{\partial \mathbf{u}}{\partial t} + \nabla \cdot (\mathbf{u}\mathbf{u}) = -\nabla p_e + \frac{1}{Re}[(1 + \nu_t)\nabla^2 \mathbf{u} + \nabla \nu_t \cdot \mathbf{D}] + \frac{1}{Fr^2}\mathbf{g} + N(\mathbf{j} \times \mathbf{b}), \tag{10}$$

$$\frac{\partial \mathbf{b}}{\partial t} = \nabla \times (\mathbf{u} \times \mathbf{b}) + \frac{1}{Re_m}\nabla^2 \mathbf{b}, \tag{11}$$

where ν_t is the turbulent viscosity, $\mathbf{D} = \frac{1}{2}[\nabla \mathbf{u} + (\nabla \mathbf{u})^T]$ is the rate-of-strain tensor, and the non-dimensional variables $\mathbf{x}/L$, tU/L, here denoted by $\mathbf{x}$ and t, are space and time, respectively. The non-dimensional fields are $\mathbf{u} = \mathbf{V}/U$, $\mathbf{b} = \mathbf{B}/B$, $p_e = p^*/\rho U^2$ and $\mathbf{g} = \mathbf{G}L/U^2$. The Reynolds number, the Froude number, the

magnetic Reynolds number, and the interaction parameter are, respectively, given by $Re = UL/\nu$, $Fr = \frac{U}{\sqrt{|G|L}}$, $Re_m = \sigma\mu_0 UL$, and $N = \sigma LB^2/(\rho U)$, where U, L, and B are characteristic velocity, length, and magnetic induction, respectively. In Eq. (10), the driving force $N(\mathbf{j} \times \mathbf{b})$ is known as the Lorentz force. The non-dimensional electric current density $\mathbf{j}$ is given by the expression

$$\mathbf{j} = \frac{1}{Re_m}\nabla \times \mathbf{b}. \tag{12}$$

For the Prandtl mixing length turbulence model

$$\nu_t = Re\ell^2(\mathbf{D} : \nabla\mathbf{u})^{1/2}, \tag{13}$$

where ℓ is the Prandtl's mixing length parameter. The Prandtl mixing length model is based upon an analogy with the Kinetic Theory of the Gases, and adds an additional turbulent viscosity determined by the velocity gradients at a given point and an additional empirical parameter, namely, Prandtl mixing length. For this, a value of $\ell = 0.003m$ was found to give good agreement with experiments in the steel industry and this values will be used in this work.

This turbulence model is the simplest of the eddy viscosity models. It is isotropic so it will fail to take any anisotropic turbulence into account which will exist at a surface and may exist due to electromagnetic induction. Even some of the more advanced models such as two-equations models share this restriction. In order to account for anisotropy it would be necessary to use either the full Reynolds stress models or Direct Numerical Simulation. These approaches would require considerably more computation and any electromagnetically induced turbulence would have to be incorporated, thus modifying these basic equations.

The magnetic induction satisfies the divergence-free constraint expressed by Eq. (9). To enforce this condition we introduce a vector potential

$$\mathbf{b} = \nabla \times \mathbf{a}, \tag{14}$$

with non-dimensional field $\mathbf{a} = \mathbf{A}/BL$.

If the oscilation of the magnetic field is much greater than the induced fluid speed, i.e. $Re_m \ll Re_\omega$, then the magnetic field is unaffected by the fluid flow, so the field calculation proceeds as if the fluid volume were a solid conductor. From the computational point of view, it means that the fluid calculation decouples from the field computation. Unfortunately, the condition $U/L \ll \omega$ leads to a viscous-magnetic boundary layer which inhibits good mixing in the body of the fluid. Thus, the industrial interest is in the case when $\omega = O(U/L)$. The fluid and magnetic fields must be solved as a coupled system.

Assuming the Coulomb gauge (see, e.g., Jackson, 1975) and using Eq. (12), we can expressed the electric current density as

$$\mathbf{j} = -\frac{1}{Re_m}\nabla^2\mathbf{a}. \tag{15}$$

With no net electric charge and non-dimensional form of the Faraday's Law (4) and of the Ohm's Law (5), we can write a diffusion equation to the vector potential $\mathbf{a}$

$$\frac{\partial\mathbf{a}}{\partial t} = \frac{1}{Re_m}\nabla^2\mathbf{a} + \mathbf{u} \times (\nabla \times \mathbf{a}). \tag{16}$$

In the two-dimensional case $\mathbf{b} = (b_x, b_y, 0)^T$ and $\mathbf{a} = (0, 0, a)^T$, the equation (16) becomes

$$\frac{\partial a}{\partial t} = \frac{1}{Re_m}\nabla^2 a - u\frac{\partial a}{\partial x} - v\frac{\partial a}{\partial y}. \tag{17}$$

Assuming a sinusoidal time dependence for a, we can write

$$a = (a_1 + ia_2)\exp(-i\omega t) \tag{18}$$

so that $\frac{\partial a}{\partial t} = -i\omega(a_1 + ia_2)\exp(-i\omega t)$ yielding

$$Re_\omega a_2 = \nabla^2 a_1 - Re_m\left(u\frac{\partial a_1}{\partial x} + v\frac{\partial a_1}{\partial y}\right), \tag{19}$$

$$-Re_\omega a_1 = \nabla^2 a_2 - Re_m\left(u\frac{\partial a_2}{\partial x} + v\frac{\partial a_2}{\partial y}\right), \tag{20}$$

where $Re_\omega = \mu_0\sigma\omega L^2$ is the shielding parameter, and a_1, a_2 are, respectively, the real and imaginary parts.

3. Initial and boundary conditions

Equations (8),(10) and (16) are coupled, non-linear, partial differential equations and, together with the eddy-viscosity model (13), are sufficient, in principle, to solve for the five unknowns u, v, p_e, a_1 and a_2 when appropriated initial and boundary conditions are specified. In this work, a staggered grid is used where the pressure p_e, the potential values a_1 and a_2 are stored at the center of a computational cell, whereas velocities u and v are stored at the cell boundaries. With this grid system, pressure boundary conditions are not needed.

For initial conditions, the values of all variables are prescribed. Two types of boundary conditions are used, namely free-surface and rigid-wall boundaries. The fluid equations are solved in the square domain. The bottom and two vertical walls are assumed to be rigid. For the top of the cavity we have a free surface.

For simplicity the material of the container will be neglected so that only a liquid/air interface need be considered. This is not an unreasonable assumption since the thickness of the container in comparison with its width is negligible and for a container made of refractory material, the permeability is close to that of free space.

3.1. Free surface

At the free-surface, we are considering that the fluid is moving into a passive atmosphere (zero-pressure) and, in the absence of surface tension forces, the normal and tangential components of the stress must be continuous across any free-surface, so that on such a surface we have (see, for example, Landau and Lifshitz, 1987)

$$\mathbf{n} \cdot (\sigma \cdot \mathbf{n}) = 0, \tag{21}$$

$$\mathbf{m} \cdot (\sigma \cdot \mathbf{n}) = 0, \tag{22}$$

where $\mathbf{n}$ and $\mathbf{m}$ are unit normal and tangent vectors to the surface, and σ is the general constitutive equation (Cauchy stress-tensor) defined as

$$\sigma = -p_e \, \mathbf{I} + \frac{1}{Re}(1 + \nu_t)\mathbf{D}, \tag{23}$$

being $\mathbf{I}$ the identity tensor. From Eqs. (21) and (22), we determine the pressure and the velocities, respectively. For more details, see Ferreira et al., 2004.

We consider that the magnetic field rapidly decays for a large container compared to the magnet site (Moffatt, 1965). It seems reasonable to assume that at the free surface the tangential components of the magnetic field are continuous i.e.

$$\mathbf{n} \times (\mathbf{b_2} - \mathbf{b_1}) = 0, \tag{24}$$

where $\mathbf{n}$ is the unit normal vector to the surface pointing outside.

3.2. Rigid wall

At the rigid walls, the no-slip conditions are applied. We assume that at the bottom of the cavity ($y = 0$ - excluding the site of the magnet), $b_x = 0$, that is $\frac{\partial a}{\partial y} = 0$. At the magnet site the value of $\mathbf{b}$ will be determined from the position and strength of the magnets. A sinusoidal distribution is chosen for the y-component of $\mathbf{b}$ at $y = 0$, i.e.

$$b_y = \frac{B_y}{B} = sin\left(\pi\frac{x}{l}\right) \tag{25}$$

where l is the lenght of the magnet. Further, in practical applications it is well known that the array of magnets exerts a magnetic field in a boundary layer close to the wall $y = 0$. As one moves away from this wall the magnetic field rapidly decays and for a large container compared to the magnet site it seems reasonable to assume that, for walls parallel to the y-axis, the tangential components of the magnetic field are continuous i.e.

$$\frac{\partial b_y}{\partial x} = 0 \qquad \text{or} \qquad \frac{\partial^2 a}{\partial x^2} = 0. \tag{26}$$

Note that $a = a_1 + ia_2$ and so these boundary conditions hold for both components. The side walls containing the molten metal are made of ceramic brick. Since this has a low conductivity, it has been neglected.

4. Solution procedure

The governing equations (8), (10), and (16) are solved with an extension of the GENSMAC methodology for turbulent MHD free surface fluid flow. The detailed information of this code for the simulation of free-surface flows without turbulence modelling is provided in Tomé and McKee, 1994. It is a finite-difference, explicit, first/second-order accurate numerical method based on a predictor-corrector scheme. By using a guessed effective pressure $\tilde{p}_e$ and an eddy-viscosity ν_t, the method consists of solving the Navier-Stokes equations (10) at the $(k+1)$ time-step for a tentative velocity field $\tilde{\mathbf{u}}$. The $\tilde{\mathbf{u}}$ is related to the true velocity field $\mathbf{u}$, at the $(k+1)$ time-step, by an auxiliary potential function ψ which is calculated from a Poisson equation, derived by imposing $\nabla \cdot \mathbf{u} = 0$ at the $(k+1)$ time-step. The effective pressure is then updated, and the procedure is repeated at each time-step. In particular, when calculating $\tilde{\mathbf{u}}$ in the first step, we employ an adaptive time-stepping routine (see Tomé and McKee, 1994). The numerical solution procedure may be summarized as follows.

It is supposed that, at a given time $t = t_0$, the velocity field $\mathbf{u}$ is known and suitable boundary conditions are given. Let $\tilde{p}_e(x, y, t)$ be an arbitrary effective pressure field, which satisfies the correct pressure condition on the free-surface. This pressure field is constructed by employing the normal-stress condition (21) at the free-surface, and it is chosen arbitrarily (for instance $\tilde{p}_e(x, y, t) = 0$) in the fluid. The updated velocity field, the effective pressure, the pontential components of the magnetic field, and the eddy-viscosity variables, at time $t = t_0 + \delta t$, are calculated by the following steps:

1. With the eddy-viscosity ν_t known at $t = t_0$ and $\tilde{\mathbf{u}}(x, y, t_0) = \mathbf{u}(x, y, t_0)$, compute an approximate velocity field $\tilde{\mathbf{u}}(x, y, t)$ from a finite-diference discretization of

$$\left.\frac{\partial \widetilde{u}}{\partial t}\right|_{t=t_0} = \left\{ -\frac{\partial(uu)}{\partial x} - \frac{\partial(uv)}{\partial y} - \frac{\partial \widetilde{p}_e}{\partial x} + \frac{1}{Re}\frac{\partial}{\partial y}\left(\frac{\partial u}{\partial y} - \frac{\partial v}{\partial x}\right) + \frac{1}{Fr^2}g_x \right.$$
$$\left. + \quad \frac{1}{Re}\left[2\frac{\partial}{\partial x}\left(\nu_t \frac{\partial u}{\partial x}\right) + \frac{\partial}{\partial y}\left(\nu_t\left(\frac{\partial u}{\partial y} + \frac{\partial v}{\partial x}\right)\right)\right] + F\right\}\Bigg|_{t=t_0}, \tag{27}$$

$$\left.\frac{\partial \widetilde{v}}{\partial t}\right|_{t=t_0} = \left\{ -\frac{\partial(vu)}{\partial x} - \frac{\partial(vv)}{\partial y} - \frac{\partial \widetilde{p}_e}{\partial y} - \frac{1}{Re}\frac{\partial}{\partial x}\left(\frac{\partial u}{\partial y} - \frac{\partial v}{\partial x}\right) + \frac{1}{Fr^2}g_y \right.$$
$$\left. + \quad \frac{1}{Re}\left[2\frac{\partial}{\partial y}\left(\nu_t \frac{\partial v}{\partial y}\right) + \frac{\partial}{\partial x}\left(\nu_t\left(\frac{\partial u}{\partial y} + \frac{\partial v}{\partial x}\right)\right)\right] + G\right\}\Bigg|_{t=t_0}, \tag{28}$$

where F and G, the components of the time-averaged Lorentz forces, are given by

$$F = N < \mathbf{j} \times \mathbf{b} >_x = \frac{-N\omega}{2\pi}\int_0^{\frac{2\pi}{\omega}} \frac{\partial a}{\partial x}\left(\frac{\partial a}{\partial t} + u\frac{\partial a}{\partial x} + v\frac{\partial a}{\partial y}\right)dt =$$
$$-\frac{N}{2}\left\{\left[\frac{\omega L}{U}a_2 + \left(u\frac{\partial a_1}{\partial x} + v\frac{\partial a_1}{\partial y}\right)\right]\frac{\partial a_1}{\partial x} + \left[\frac{-\omega L}{U}a_1 + \left(u\frac{\partial a_2}{\partial x} + v\frac{\partial a_2}{\partial y}\right)\right]\frac{\partial a_2}{\partial x}\right\}, \tag{29}$$

$$G = N < \mathbf{j} \times \mathbf{b} >_y = \frac{-N\omega}{2\pi}\int_0^{\frac{2\pi}{\omega}} \frac{\partial a}{\partial y}\left(\frac{\partial a}{\partial t} + u\frac{\partial a}{\partial x} + v\frac{\partial a}{\partial y}\right)dt =$$
$$-\frac{N}{2}\left\{\left[\frac{\omega L}{U}a_2 + \left(u\frac{\partial a_1}{\partial x} + v\frac{\partial a_1}{\partial y}\right)\right]\frac{\partial a_1}{\partial y} + \left[\frac{-\omega L}{U}a_1 + \left(u\frac{\partial a_2}{\partial x} + v\frac{\partial a_2}{\partial y}\right)\right]\frac{\partial a_2}{\partial y}\right\}. \tag{30}$$

It can be shown (see, for example, Ferreira et al., 2004) that $\tilde{\mathbf{u}}(x, y, t)$ possesses the correct vorticity at time t but does not satisfy (8), in general. By writting

$$\mathbf{u}(x, y, t) = \widetilde{\mathbf{u}}(x, y, t) - \nabla \psi(x, y, t) \tag{31}$$

and imposing

$$\nabla^2 \psi(x, y, t) = \nabla \cdot \widetilde{\mathbf{u}}(x, y, t), \tag{32}$$

a velocity field is obtained in which the vorticity and mass are conserved;

2. Solve the Poisson equation (32) for ψ. The appropriate boundary conditions for this elliptic equation are homogeneous Dirichlet-type on the free-surface and homogeneous Neumann-type on fixed boundaries. These are treated in a similar way as in the GENSMAC code;

3. Calculate the velocity field $\mathbf{u}(x, y, t)$ from (31);

4. Compute the effective pressure. It can be shown (see Ferreira et al., 2004) that the effective pressure field is given by

$$p_e(x, y, t) = \tilde{p}_e(x, y, t) + \psi(x, y, t)/\delta t; \tag{33}$$

5. Compute the potential components a_1 and a_2 from a finite-difference approximation of (18) and (19);

6. Update the eddy-viscosity ν_t from (13);

7. Particle movement. The last step in the calculation involves the movement of the marker particles to their new positions. These are virtual particles (without mass, volume, or other properties), whose coordinates are stored and updated at the end of each cycle by solving the ordinary differential equations

$$\frac{dx}{dt} = u \quad \text{and} \quad \frac{dy}{dt} = v \tag{34}$$

by Euler's method. This provides a particle with its new coordinates, allowing us to determine whether or not it has moved into a new computational cell;

8. Update the boundary conditions and go back to the first step.

5. Discretization

In the solution procedure outlined above, the differential equations are discretized in time and space in precisely the same manner for all dependent variables. The temporal derivatives are discretized using the Euler's method, while the spatial derivatives are evaluated using specific finite-differences on a uniform staggered grid system. The non-linear terms in F and G of (29) and (30) are, respectively, approximated using the first order upwind discretization. The others non-linear terms are approximated by the Variable-Order Non-Oscillatory Scheme (VONOS) of Varonos and Bergeles, 1998, which satisfy the Convection Boundedness Criterion (CBC) formulated by Gaskell and Lau, 1998. All the other derivatives are approximated using standard second-order central-difference formulation. The Poisson equation (32) is discretized using the usual five-point Laplacian operator, and the corresponding symmetric-positive definite linear system is solved by the conjugate-gradient method.

5.1. Discretization of the magnetic field equations

Equations (19) and (20) are applied at the center of the cell. The approximations for the velocities u and v at the cell center will be denoted by u_{ij} and v_{ij} respectively. These values are interpolated by taking the averages over the face values.

For a typical interior grid point the discretization of (18) produces

$$C_{i-1,j}^1 a_{i-1,j}^1 + C_{ij}^1 a_{i,j}^1 + C_{i+1,j}^1 a_{i+1,j}^1 + C_{i,j-1}^1 a_{i,j-1}^1 + C_{i,j+1}^1 a_{i,j+1}^1 = Re_\omega a_{i,j}^2, \tag{35}$$

where $a_{ij}^k \simeq a_k(x_i, y_j), k = 1, 2$ and the coefficients C^1 are given by

$$C_{ij}^1 = -\frac{2}{h_x^2} - \frac{2}{h_y^2} - Re_m \frac{u_{ij} - |u_{ij}|}{2h_x} - Re_m \frac{v_{ij} - |v_{ij}|}{2h_y}, \tag{36}$$

$$C_{i-1,j}^1 = \frac{1}{h_x^2} - Re_m \frac{u_{ij} + |u_{ij}|}{2h_x}, \tag{37}$$

$$C_{i+1,j}^1 = \frac{1}{h_x^2} - Re_m \frac{u_{ij} - |u_{ij}|}{2h_x}, \tag{38}$$

$$C_{i,j-1}^1 = \frac{1}{h_y^2} - Re_m \frac{v_{ij} + |v_{ij}|}{2h_y}, \tag{39}$$

$$C^1_{i,j+1} = \frac{1}{h_y^2} - Re_m \frac{v_{ij} - |v_{ij}|}{2h_y}. \tag{40}$$

A similar equation can be derived from the discretization of (19), which is written

$$C^2_{i-1,j}a^2_{i-1,j} + C^2_{ij}a^2_{i,j} + C^2_{i+1,j}a^2_{i+1,j} + C^2_{i,j-1}a^2_{i,j-1} + C^2_{i,j+1}a^2_{i,j+1} = -Re_\omega a^1_{i,j}. \tag{41}$$

where the coefficients C^2 are obtained as C^1. Using the row ordering for the unknowns $a^1_{i,j}$ and $a^2_{i,j}$, equations (35) and (41) can be rewritten as two coupled linear systems:

$$\begin{pmatrix} M^1 & -Re_\omega I \\ Re_\omega I & M^2 \end{pmatrix} \begin{pmatrix} A^1 \\ A^2 \end{pmatrix} = \begin{pmatrix} a \\ b \end{pmatrix} \tag{42}$$

where A^1 and A^2 are the vectors of the unknowns, M^1 and M^2 are the discretization matrices and a and b are vectors representing the boundary conditions. The linear system (42) is large, sparse and non-symmetric. It is solved by the biconjugate gradient method.

6. Numerical results

A two-dimensional square cavity in a stirring application with free-surface on the top was simulated. For this free surface flow, no comparision with experimental data is presented because the authors did not find the similar data in the literature. The material properties of the liquid metal used in the computations are density $\rho = 7,070 kg/m^3$, kinematic viscosity $\nu = 0.886.10^{-6} m^2/s$, magnetic permeability $\mu_0 = 4\pi.10^{-7} H/m$, and electrical conductivity $\sigma = 715,000\Omega/m$. The magnetic field strength is $B = 0.03T$ with frequency $\omega = 62.832 s^{-1}$. Computations are performed on mesh 20×20 computational cells ($\delta x = \delta y = 0.01m$). In these simulations, the characteristic velocity $U = B(\frac{\sigma}{\rho\omega})^{1/2}\omega L = 0.4782 m/s$ and the characteristic lenght $L = 0.2m$ were used. The non-dimensional groups are: Reynolds number $Re = 107,900$, Froude number $Fr = 0.3414$, magnetic Reynolds number $Re_m = 0.0859$, shielding parameter $Re_\omega = 2.25817$, and interaction parameter $N = 0.0381$.

In the sequel, various diagrams are presented depicting the fluid flow behaviour for different positioning of the magnets at the non-dimensional time $t = 6.5$. Figure (1) shows the simulation of the stirring metal in a cavity with one magnet on the bottom. The magnetic field rapidly decays when one moves away from the bottom wall. This figure shows the pressure, components of velocity (u, v) and the real part of the magnetic vector potential a_1. This alternating field has a sinusoidal magnetic distribution. Results are also shown for two poles configuratiom in Fig. (2). In this figure the same diagrams are displayed, pressure, (u, v), and a_1. There is an overlap of the main flow from the separate poles. There are more pronunciated effects of the magnet distribution and of the free surface.

Now the convergence test of the numerical solution for the previous problem is reported. This is performed under the mesh refinement of the computational mesh. Figure (3) shows the time-dependent free surface profile from computations with the sequence of 20×20, 40×40 and 80×80 computational cells. One can see, from this figure, that the computed free surface of the fluid on the 20×20 and 40×40 meshes converges to the computed free surface on the 80×80 mesh, indicating grid independence of numerical results.

7. Conclusions

The velocity-coupled Lorentz force together with the Prandtl mixing-length turbulent Navier-Stokes equations for two-dimensional electromagnetically-driven stirring has been solved. The influence of coupling effects at low frequency has been observed for alternating magnetic fields. The Lorentz body force for a simple one-dimensional model has an exponential decay in the interior of a conducting medium, dependent upon the frequency of the applied magnetic field (Moffatt, 1965). This influences the overall distribution of vorticity-production within the fluid flow.
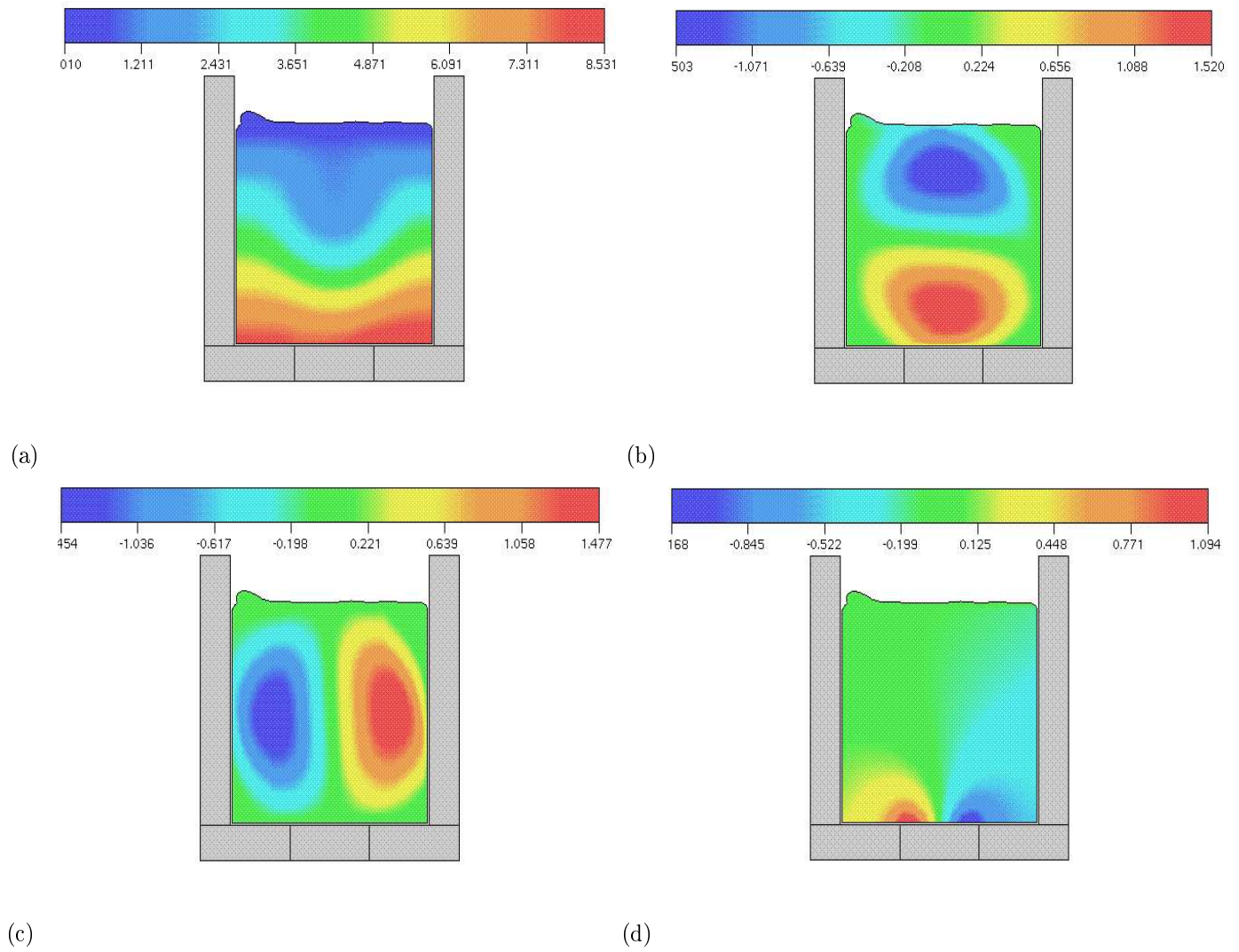
8. Acknowledgements

(a)

(b)

(c)

(d)

Figure 1: One magnet on bottom ($t = 6.5$): (a) pressure; (b) u velocity; (c) v velocity; (d) a_1 real part of the magnetic vector potential.
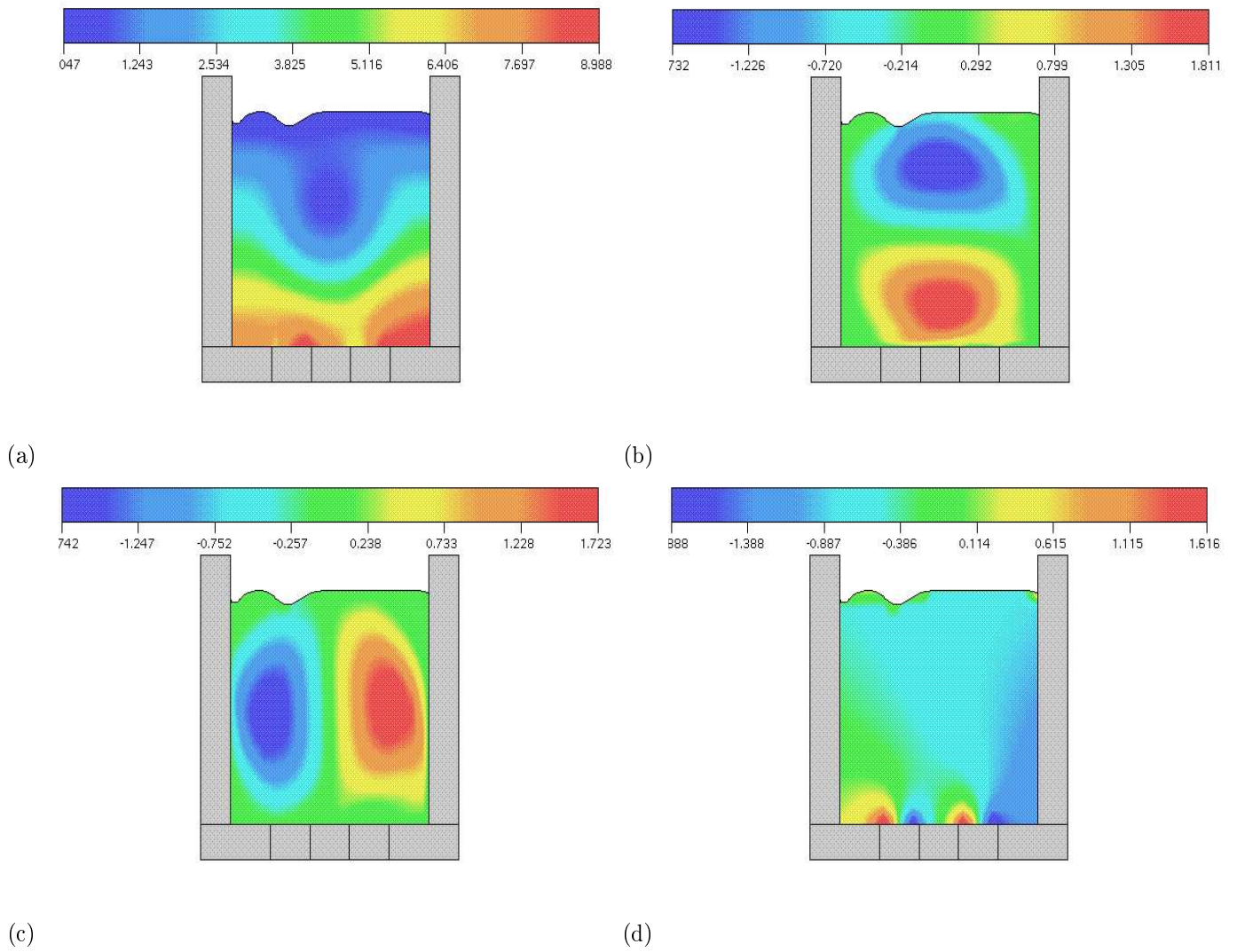
(a)

(b)

(c)

(d)

Figure 2: Two magnets on bottom ($t = 6.5$): (a) pressure; (b) u velocity; (c) v velocity; (d) a_1 real part of the magnetic vector potential.
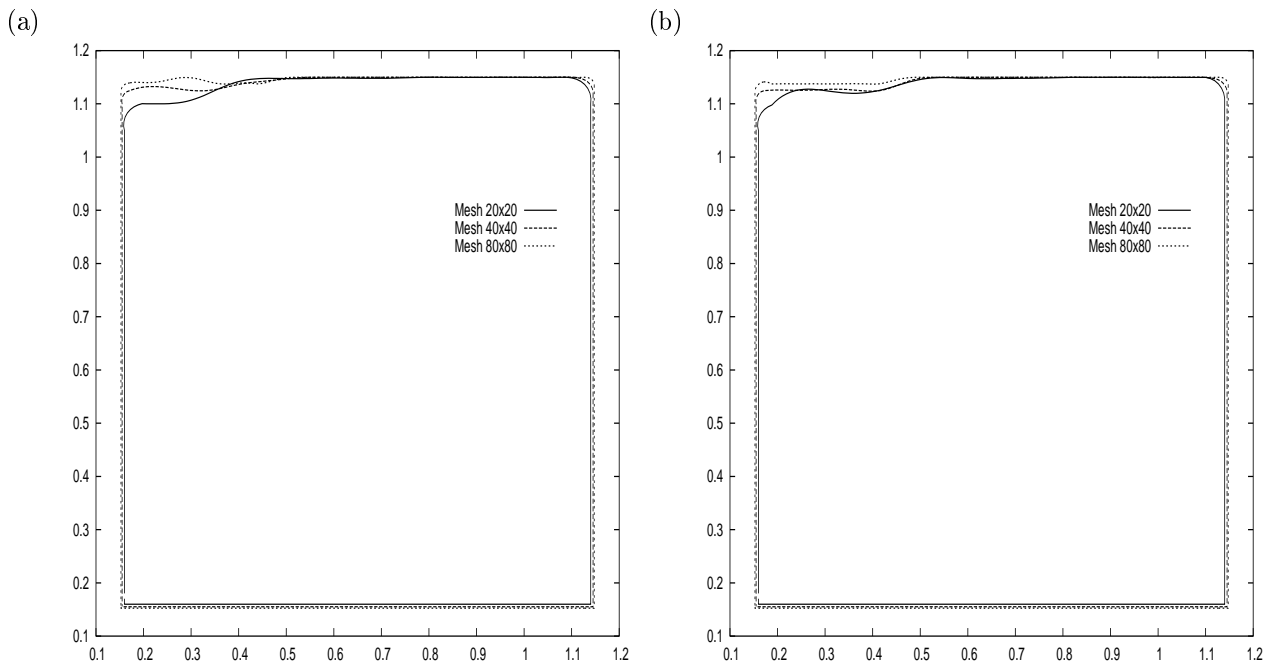
(a)
(b)

Figure 3: Transient free surface profile using three meshes: (a) $t = 0.5$s and (b) $t = 1.0$s

9. References

Davidson, P. A. and Hunt, J. C. R., 1987, Swirling Recirculating Flow in a Liquid-Metal Column Generated by a Rotating Magnetic Field, "J. Fluid Mech.", Vol. 185, pp. 67–106.

Ferreira, V. G., Mangiavacchi, N., Tomé, M. F., Castelo, A., Cuminato, J. A., and McKee, S., 2004, Numerical Simulation of Turbulent Free Surface Flow with Two-Equation $\kappa - \varepsilon$ Eddy-Viscosity Models, "Int. J. Numer. Meth. Fluids", Vol. 44, pp. 347–375.

Gaskell, P. H. and Lau, A. K. C., 1998, Curvature-Compensated Convective Transport: SMART, A New Boundedness Preserving Transport Algorithm, "Int. J. Numer. Meth. Fluids", Vol. 8, pp. 617–641.

Jackson, J. D., 1975, "Classical Electrodynamics", John Wiley, New York, NY, 848 p.

Landau, L. D. and Lifshitz, E. M., 1987, "Fluid Mechanics", Pergamon Press, Oxford, England, 539 p.

Moffatt, H. K., 1965, On Fluid Flow Induced by a Rotating Magnetic Field, "J. Fluid Mech.", Vol. 22, pp. 521–528.

Nigam, G. D., 1969, Flow of a Fluid in a Spherical Container in the Presence of a Rotating Magnetic Field, "J. Math. Phys. Sci.", Vol. 3, pp. 205–222.

Northrup, E. F., 1907, Some Newly Observed Manifestations of Forces in the Interior of an Electric Conductor, "Phys. Rev.", Vol. XXIV, pp. 474–497.

Richardson, A. T., 1974, On the Stability of a Magnetically Driven Rotating Fluid Flow, "J. Fluid Mech.", Vol. 63, pp. 593–605.

Sneyd, A. D., 1971, Generation of Fluid Motion in a Circular Cylinder by an Unsteady Applied Magnetic Field, "J. Fluid Mech.", Vol. 49, No. 4, pp. 817–827.

Sneyd, A. D., 1979, Fluid Flow Induced by a Rapidly Alternating or Rotating Magnetic Field, "J. Fluid Mech.", Vol. 92, pp. 35–51.

Tomé, M. F. and McKee, S., 1994, GENSMAC: A Computational Marker and Cell Method for Free Surface Flows in General Domains, "J. Comput. Phys.", Vol. 110, No. 1, pp. 171–186.

Varonos, A. and Bergeles, G., 1998, Development and Assessment of a Variable-order Non-oscillatory Scheme for Convection Term Discretization, "Int. J. Numer. Meth. Fluids", Vol. 26, No. 1, pp. 1–16.